AIP | Review of Scientific Instruments

Improving the reliability of multiplexed fiber optic low-coherence interferometric sensors by use of novel twin-loop network topologies

Jun Yang, Libo Yuan, and Wei Jin

Citation: Rev. Sci. Instrum. **78**, 055106 (2007); doi: 10.1063/1.2735564
View online: http://dx.doi.org/10.1063/1.2735564
View Table of Contents: http://rsi.aip.org/resource/1/RSINAK/v78/i5
Published by the American Institute of Physics.

Improving the reliability of multiplexed fiber optic low-coherence interferometric sensors by use of novel twin-loop network topologies

Jun Yang and Libo Yuan[a)]
Photonics Research Center, College of Science, Harbin Engineering University, Harbin 150001, People's Republic of China

Wei Jin
Department of Electrical Engineering, The Hong Kong Polytechnic University, Hong Kong, People's Republic of China

(Received 8 July 2006; accepted 16 March 2007; published online 11 May 2007)

Novel twin-loop network topologies for multiplexing fiber optic low-coherence reflectometric sensors are proposed and theoretically analyzed. The sensing fibers are made by connecting segments of standard single-mode fibers with partial reflections at the fiber joints and are completely passive. Absolute length measurement can be made for each segment of the sensing fiber so that strain or temperature distribution along the entire sensing fiber can be derived. It is expected that novel topologies would help as to improve the reliability of the sensor network by providing multiple accesses to each of the sensing segment so that most of the sensing segments can still be interrogated even when one or more point breakages occur along the transmission fibers. A nine-sensor twin-loop sensing network was constructed and experimentally tested by use of a Michelson low-coherence interferometer, and the results obtained agree with our theoretical prediction. The novel network topologies may be used for large-scale smart structure applications where breakages of transmission fibers may occur during the stages of sensor imbedding, installation, and structure-in-service cycles. © *2007 American Institute of Physics.*
[DOI: 10.1063/1.2735564]

I. INTRODUCTION

In most multiplexed or distributed optical fiber sensing systems, sensing elements are typically fabricated along or connected in serial to a single fiber optic transmission line. Examples of these systems are fiber Bragg grating sensors,[1,2] optical time domain reflectometry sensors,[3,4] and distributed or quasidistributed sensors based on optical low-coherence reflectometry.[5–7] These systems, however, have one common drawback: the damage or the breakage of fiber at a single location along the sensing or the transmission fiber would cause part and even the whole system failure. This is especially critical for smart structure applications, where the sensing/transmission fibers are embedded within structures and the repair is often impractical. These problems require the sensor system designers to consider, at a network rather than independent device level, multiplexing and networking techniques to ensure sufficient redundancy for the purpose of system reliability.[8,9]

The purpose of the present work is to improve the reliability without significantly comprising the multiplexing capacity of the multiplexed or quasidistributed low-coherence reflectometry sensor systems. Low-coherence or white light interferometry, as a technique employing low-coherence broadband light sources, has been a very active area of researches in recently years. The idea of using a short coherence length source to separate the signals returning from a series of sensors was first published by Al-Chalabi *et al.*[10] Brooks *et al.* proposed a series of Mach-Zehnder interferometers and ladder coherence multiplexing scheme.[11] Gusmeroli reported a low-coherence polarimetric sensor array multiplexed on the fiber line.[12] Sorin and Baney[13] and Inaudi *et al.*[14] further developed and simplified the quasidistributed low-coherence fiber optic sensor array based on a scanning Michelson interferometer. We have previously demonstrated bidirectional interrogation of low-coherence interferometric sensors by connecting a serial array of sensors into a loop topology. This topology allows normal interrogation of most of the sensors even when the connection or transmission fiber is broken at a particular location and the system reliability is hence enhanced. In this article, we report significant improvement of redundancy or reliability of the low-coherence interferometric sensors by using twin-loop topologies. The use of various twin-loop topologies, i.e., fiber Sagnac loop and resonator combinations, allows multiple interrogation of the same sensor and hence improve redundancy and system reliability and avoids the whole system failure even in the case of single or multiple breakages of transmission fibers. These twin-loop network topologies are expected to be useful for applications in large-scale structure condition monitoring.

II. TWIN-LOOP NETWORK TOPOLOGIES

The twin-loop network topologies are extensions of the one-loop topology, in which segments of sensing fibers are

[a)]FAX: 86-451-82519850; electronic mail: lbyuan@vip.sina.com

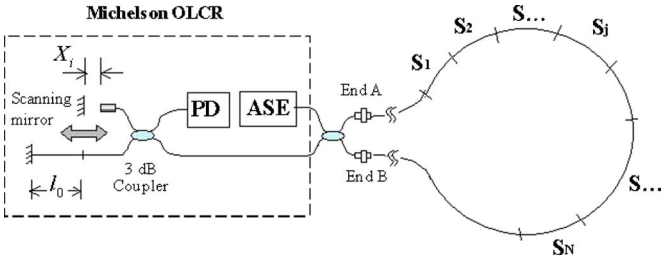

FIG. 1. (Color online) Schematic of multiplexed fiber optic sensor array with one-loop topology.

jointed in serial and further connected to form a fiber Sagnac loop to allow for bidirectional interrogation of each of the sensing segments (Fig. 1).[15,16] The basic building blocks of the twin-loop systems are a fiber Sagnac loop and a fiber ring-resonator loop, from which six possible twin-loop topologies (Fig. 2), corresponding to various combinations of Sangac and resonator loops, may be configured. Compared with the single-loop topology, one of the advantages of the twin-loop configuration is the enhanced multiplexing capacity. It provides more redundancy for the sensing system.

III. INTERROGATION OF MULTIPLEXED SENSOR ARRAY

The sensor array in a twin-loop topology can be interrogated by using the low-coherence reflectometry principle based on a scanning optical fiber Michelson interferometer (Fig. 3). The principle of operation may be explained by use of the serial and parallel Sagnac-resonator twin-loop combinations, as shown, respectively, in Figs. 3(a) and 3(b).

Low-coherence light from an erbium-doped fiber amplified spontaneous emission (ASE) source is launched via an isolator into the sensor array through the use of a fused 3 dB directional coupler. The sensing fiber segments are connected as shown in Figs. 3 and 4 to form a twin-loop network. Light is reflected by in-line reflectors formed by a small air gap at the joint between the two adjacent sensing fiber segments, and the reflected light signal from the twin-loop sensor array is then coupled into the optical low-coherence reflectometer (OLCR). Inside the OCLR, a second 3 dB coupler splits the

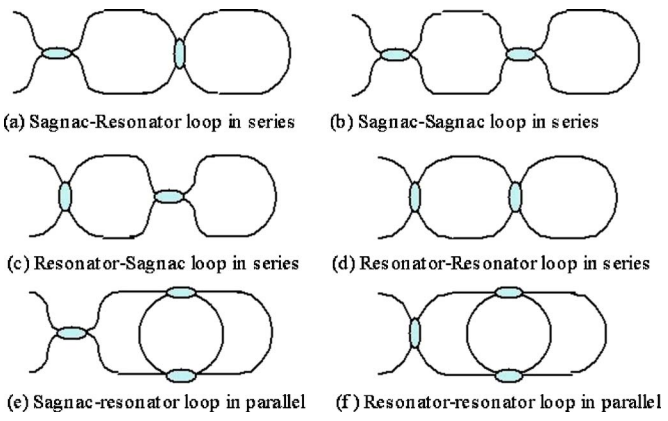

FIG. 2. (Color online) Possible twin-loop network topologies. (a) Sagnac-resonator in serial, (b) Sagnac-Sagnac in serial, (c) resonator-Sagnac in serial, (d) resonator-resonator in serial, (e) Sagnac-resonator in parallel, and (f) resonator-resonator in parallel.

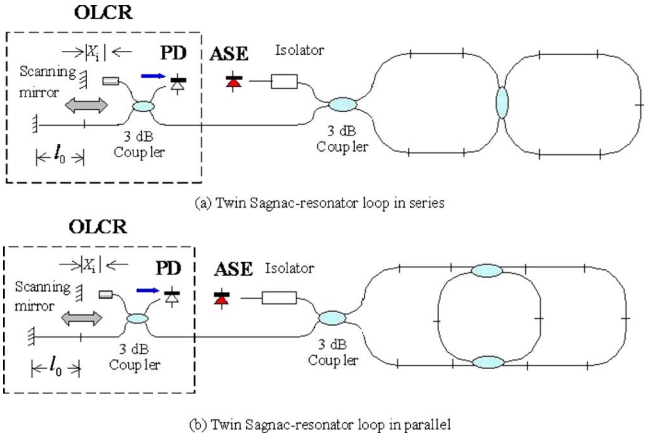

FIG. 3. (Color online) An example of twin-loop network interrogated by scanning low-coherence Michelson interferometer. (a) Sagnac-resonator in serial and (b) Sagnac-resonator in parallel.

returned light signal from the sensor array, and the signal in the lower arm of the coupler is reflected directly by a mirrored fiber end. The signal in upper arm leads to the fiber optic collimator and reflected by a scanning mirror. The two reflected signals are combined at the 3 dB coupler and detected by a photodetector (PD).

The reflectivity of the in-line reflectors is typically very small and on the order of 1% or less. The sensor gauge lengths, that are the lengths (l_i) of the sensing segment S_i ($i=1,2\ldots,N$) between the adjacent reflectors, can be any value as long as their differences are not larger than the scanning range of the OLCR system. In our experiments, l_i has been chosen to be around 500 mm and the initial optical path difference (l_0) of the OLCR is chosen to be approximately the same in order to match the path lengths of the sensing segments. The length difference between any two fiber sensing segments is within 270 mm, corresponding to less than 400 mm in air which is the maximum scanning range of our OLCR system. Such a selection of system parameters guarantees that the path length of the interrogation Michelson interferometer matches to each pairs of the re-

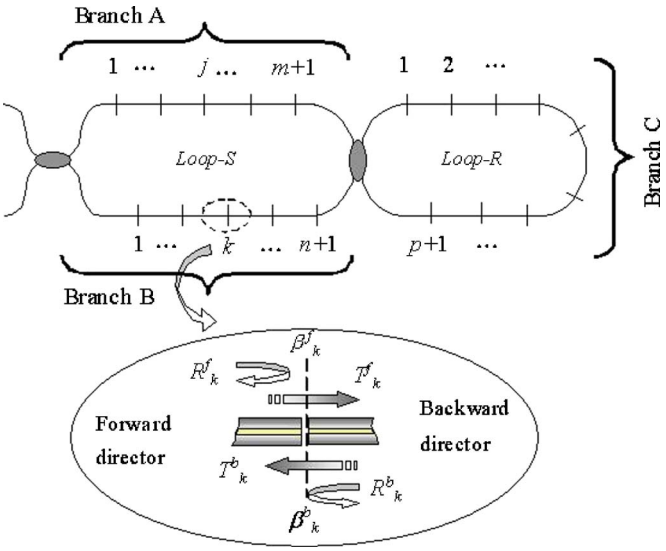

FIG. 4. (Color online) Signal analyses in parallel Sagnac-resonator network.

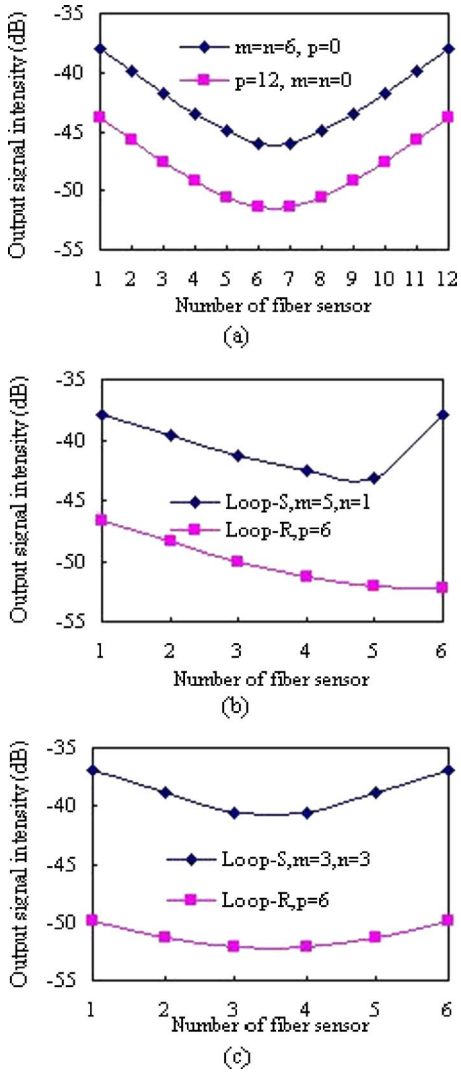

FIG. 5. (Color online) Signal outputs of a 12-sensor twin-loop network with different sensor numbers in loop S and loop R. (a) Upper curve: no sensor in loop R and six sensors in branches A and B of loop S, lower curve: no sensor in loop S and 12 sensors in in loop R; (b) five in branch A, one in branch B of loop S, and six in loop R, (c) three in branch A, three in branch B of loop S, and six in loop R.

flected signals generated from the adjacent reflectors and hence the generation of effective interference signals for each of the sensing segments.

The multiplexed sensing system may be regarded as the tandem of a Michelson demodulator interferometer and a series of Fieazu interferometers formed by the reflected beams from the two joints at the ends of each sensing segment. The optical path difference (OPD) of the Michelson interferometer is adjusted through the use of a scanning mirror to match and trace the change of the fiber length in each sensing segment. When the OPD of the Michelson interferometer is matched to the gauge length of a particular sensing segment, a white light fringe pattern is produced. The central fringe, which is located in the center of the fringe pattern and has the highest amplitude peak, corresponds to the exact OPD match for that sensor. The optical path matching condition for sensing segment l_k is given by

$$n_0 l_0 + X_k = n_0 l_k, \tag{1}$$

where n_0 is the effective refractive index of the fiber mode, l_0 is the initial OPD of the Michelson demodulation interferometer, and X_k is the distance between scanning mirror and the fiber collimator. As the OPD $(n_0 l_k)$ of the fiber sensor is modulated by the ambient perturbation, for instance strain or temperature, they may be monitored through OPD measurement by recording the shift of in the position of the scanning mirror (ΔX_k) that corresponds to the peak of the center fringe. Form Eq. (1), we obtain

$$\Delta X_k = \Delta(n_0 l_k). \tag{2}$$

To avoid overlap of the interference fringe pattern, the gauge lengths of the sensing segments are chosen to satisfy the following conditions:

$$|l_i - l_j| \geqslant L_c,$$

$$|l_i - l_j| \leqslant D_s, \tag{3}$$

where L_c is the coherence length of the ASE source and D_s is the maximum scanning distance of the moving mirror.

TABLE I. Multiplexing capacity versus light source power for various twin-loop sensor networks.

Light source power (mW)		0.05	0.2	1.0	3.0	5.0
Sensor number $m=n$	$m=n=0$ $N_{max}=p$	5	10	16	20	24
	$p=0$ $N_{max}=m+n$	8	16	20	22	24
Sensor number $m \neq n$ $m=0$	$2n=p$ $N_{max}=n+p$	4	9	15	16	18
	$n=p$ $N_{max}=n+p$	5	10	17	18	22
	$n=2p$ $N_{max}=n+p$	8	14	24	26	28

IV. OUTPUT SIGNAL ANALYSIS

We take the serially connected Sagnac-resonator twin-loop case (Fig. 4) as an example to evaluate the magnitude of the output signal from individual sensors in the network. According to the locations of the sensors in the array, we

TABLE II. Gauge lengths of the experimental nine-sensor system and locations of the interference fringe peaks in terms of positions of the scanning mirror.

Sensor label S_k	S_1	S_2	S_3	S_4	S_5	S_6	S_7	S_8	S_9
Gauge length l_k (mm)	496.84	497.39	499.15	501.91	503.21	504.27	505.34	506.11	506.54
Scanning mirror position (label)	X_1	X_2	X_3	X_4	X_5	X_6	X_7	X_8	X_9
Scanning mirror position value (mm)	125.16	125.96	128.52	132.56	134.46	136.00	137.56	138.68	139.32
Initial OPD of the Michelson interferometer l_0 (mm)					411.12				

may divide them into three arrays located, respectively, in branches A and B in the Sagnac loop (loop S) and branch C in the resonator loop (loop R). The numbers of sensors of these arrays are m, n, and p for branches A, B, and C, and they are defined by, respectively, $m+1$, $n+1$, and $p+1$, partial reflectors are labeled in Fig. 4. The total number of sensors is $N=m+n+p$.

As the mirror in the interrogator interferometer (Fig. 3) is scanned, there will be N groups of interference fringe patterns, corresponding to the matching of OPD of the interrogator interferometer to that of the N sensing segments in the twin loop. The peak fringe intensity I_j at the photodetector corresponding to the jth sensor, which is due to the coherent mixing between the reflected waves from the jth and $(j+1)$th reflectors, may be expressed as follows:

For sensors in branch A,

$$I_j = I_j^f + I_j^b = I_0\left(\frac{\alpha^4}{8}\right)\sqrt{R_f R_M \eta(X_j)}\left\{\left[\prod_{i=2}^{j}(T_i\beta_i)^2\right]\sqrt{R_j R_{j+1}(T_j\beta_j)^2} + \frac{(\alpha/2)^2\left[\prod_{i=1}^{m+1}(T_i\beta_i)\right]^2}{\left\{1-(\alpha/2)\left[\prod_{i=1}^{p+1}(T_i\beta_i)\right]^2\right\}^2}\left[\prod_{i=j+2}^{n+1}(T_i\beta_i)^2\right]\sqrt{R_j R_{j+1}(T_{j+1}\beta_{j+1})^2}\right\}. \quad (4)$$

For sensor in branch B,

$$I_j = I_j^f + I_j^b = I_0\left(\frac{\alpha^4}{8}\right)\sqrt{R_f R_M \eta(X_j)}\left\{\left[\prod_{i=2}^{j}(T_i\beta_i)^2\right]\sqrt{R_j R_{j+1}(T_j\beta_j)^2} + \frac{(\alpha/2)^2\left[\prod_{i=1}^{n+1}(T_i\beta_i)\right]^2}{\left\{1-(\alpha/2)\left[\prod_{i=1}^{p+1}(T_i\beta_i)\right]^2\right\}^2}\left[\prod_{i=j+2}^{m+1}(T_i\beta_i)^2\right]\sqrt{R_j R_{j+1}(T_{j+1}\beta_{j+1})^2}\right\}. \quad (5)$$

For sensors in branch C,

$$I_j = \frac{I_0(\alpha/2)^6\sqrt{R_f R_M \eta(X_j)}}{\left\{1-\alpha/2\left[\prod_{i=1}^{p+1}(T_i\beta_i)\right]^2\right\}^2}\left\{\left[\prod_{i-1}^{n+1}(T_i\beta_i)\right]^2\sqrt{R_j R_{j+1}(T_j\beta_j)^2}\left[\prod_{i=2}^{j}(T_i\beta_i)^2\right] + \left[\prod_{i-1}^{m+1}(T_i\beta_i)\right]^2\sqrt{R_j R_{j+1}(T_{j+1}\beta_{j+1})^2}\left[\prod_{i=j+2}^{m+1}(T_i\beta_i)^2\right]\right\}, \quad (6)$$

where I_j^f and I_j^b are, respectively, due to the interference of the reflective beams from the forward and backward directions, I_0 represents the light intensity coupled into the optical fiber from the ASE source, α is the insertion loss of the 3 dB couplers which are assumed to be the same for the same couplers, β_i represents the excess loss associated with sensor i, which is mainly due to the connection loss between the sensing segments, T_i and R_i are, respectively, the transmission and reflection coefficients of the ith partial reflector, and T_i is, in general, smaller than $1-R_i$ because of the loss factor β_i. It should be mentioned, for the same sensing segment, that value of the excess loss, transmission, and reflection coefficients could be slightly different for the forward and backward directions, however, for simplicity, we assume they are the same, i.e., $T_i^f=T_i^b=T_i$, $R_i^f=R_i^b=R_i$, and $\beta_i^f=\beta_i^b=\beta_i$. $\eta(X_i)$ is the loss associated with the scanning mirror and collimating optics and is a function of the scanning mirror position X_j. R_f and R_M are the reflectivities of the mirrored fiber end and the scanning mirror, respectively.

Based on Eqs. (4)–(6), we calculated the output signal intensities of several 12-sensor networks based on the serial Sagnac-resonator twin-loop topology. For the convenience of calculation, we neglect the excess insertion loss of the 3 dB couplers ($\alpha=0$) and assumed that $\beta_i=0.9$, $R_i=1\%$, $T_i=0.89$,

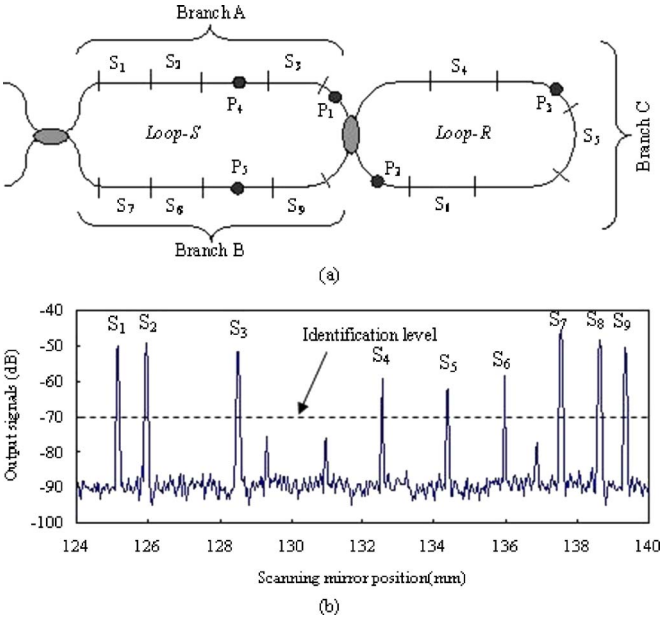

FIG. 6. (Color online) (a) Schematic of the nine-sensor network used to experimentally test the reliability of the twin-loop network; (b) signal outputs from the nine-sensor network. The fiber segments labeled with S_1, S2, S_9 representing nine sensors and the fiber lines not labeled are connecting fibers. P_1, P_2, P3, P_4, and P_5 indicate the locations of the five break points used in our experiment. Disconnecting FC-PC connectors simulates fiber breakages.

and $\eta(X_i)=1/4$ or 6 dB $(i=0,1,2,\ldots,N)$. The reflectivities of mirrored fiber end and the scanning mirror in the Michelson interferometer are taken as 80% and 50%, respectively, and the power coupled into the sensor array is taken as $I_0=1$ mW. Figure 5 shows the output signal intensities for different numbers of sensors distributed in branches A, B, and C. Figure 5(a) shows the results for a total of 12 sensors distributed in either loop S or loop R. The signal levels for the sensors in the resonator are reduced by ~6 dB due to the 3 dB coupler used to bridge loop S with loop R. Figures 5(b) and 5(c) show the results for cases of six sensors in branches A and B of loop S and six sensors in loop R. The difference between the signal levels for the sensors from the two loops levels is further increased because the sensor outputs in loop R are doubly reduced by the losses in the sensors in loop S and insertion losses of the 3 dB coupler.

V. EVALUATION OF MULTIPLEXING CAPACITY

The number of sensors that may be multiplexed in the network is by the moving range of the scanning mirror and the minimum detectable power level of the photodetector as compared with the input power level. Assuming that dynamic ranges of the sensors are less than 1 mm and an additional of 2 mm difference in the gauge lengths of the adjacent sensors in order to avoid overlap of signals from different sensors, a 400 mm scanning distance of moving mirror would give a maximum sensor number of about 85. However, it is found that the sensor numbers in the twin-loop fiber sensor network are more likely to be limited by the power budget requirement. The fraction of the source power coupled into the fiber network is distributed over the sensor arrays in each of the sensing branches. Each sensing element dissipates a certain amount of power due to various loss mechanisms such as insertion at the fiber joints. Assume that the minimum detectable power level of the photodiode is $I_{\min}$, then the maximum number of the total fiber optic sensors may be evaluated by using

$$I_j \geqslant I_{\min}, \tag{7}$$

where I_j is the output signal level of sensor j, as given in Eqs. (5)–(7). For our experimental system, the minimum detectable intensity level is ~2 nW (−57 dBm). The calculated maximum number of sensors or the multiplexing capacity for various input power levels and for different relative distributions of sensors in branches A, B, and C are given in Table I.

VI. EXPERIMENTS AND RESULTS

Experiments were carried by using a setup shown in Fig. 3(a). The light power is an Er-doped ASE source with center wavelength of 1550 nm and a bandwidth of 35 nm. The power level coupled into the sensor network is about 1 mW. The moving range of the scanning mirror is 400 mm in air and the average insertion losses in scanning system is about 5 dB with the fluctuation less than 0.2 dB. A total of nine fiber sensors were connected into the twin-loop network with detailed distributions of sensors in loop S and loop R are shown in Fig. 6(a). The gauge length of the nine sensors, the initial OPD of the Michelson interrogation interferometer, and the positions of the scanning mirrors as determined from Eq. (1) are summarized in Table II. The actual output signal as function of the scanning mirror position is plotted in Fig. 6(b). The positions of the interference fringe peaks agree with the results shown in Table II and the signal intensity distribution approximately agree with the theoretical results obtained from on Eqs. (4)–(6).

A series of damage-simulation experiments was carried out to examine the robustness of the output signals from the twin-loop sensors network. The locations of the five chosen fiber breakpoints are marked in Fig. 6(a). Figures 7(a)–7(e) show the recorded output signals when single points of P_1, P_2, P_3, P_4, and P_5 were broken. It can be seen that the nine sensors are still functioning well with locations of the signal peaks not being affected and the peak intensities being slightly less than the original ones, as shown in Fig. 6(b).

Figures 8(a)–8(g) show the test results when an arbitrary combination of two points is broken at the same time. For this case, the sensor information may or may not be lost and the degree of information lost depends on the exact locations of the broken points. When P_1 and P_2 [Fig. 8(a)] are broken, most sensor signals are not affected although the magnitudes of the signal intensities of sensor S_4, S_5, and S_6 are reduced; however, they are all above the set identification level of −70 dB and hence have no effect on the measurement results. This is expected because all the sensors are still connected to the source and the detector by at least one fiber and the signals from all the sensors can still be detected. Similarly, when P_2 and P_4 [Fig. 8(f)] are broken, all the sensor signals are still above the identification level although signal levels from S_3, S_4, S_5, and S_6 are reduced. For the case where P_1 and P_4 are broken, signal from S_3 is lost [Fig. 8(c)] because it is completely cut off but all other sensors signals

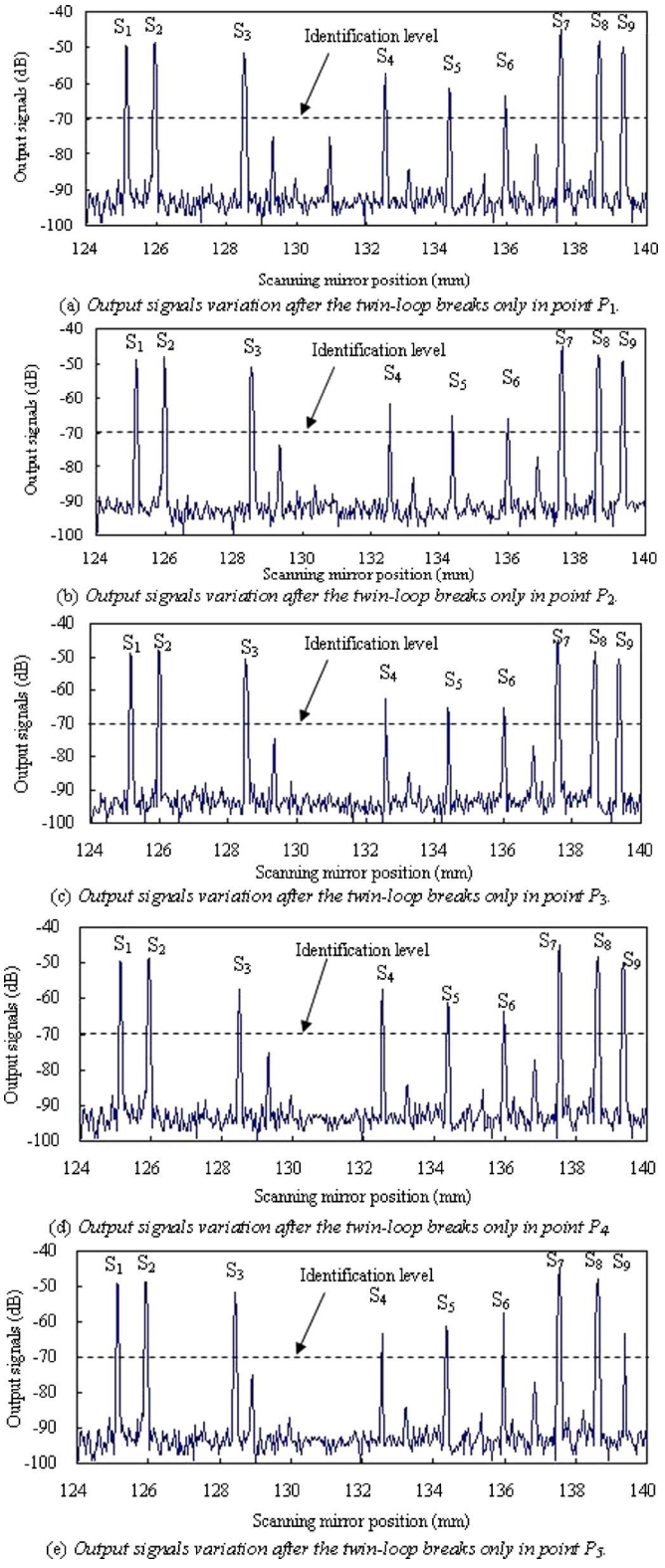

FIG. 7. (Color online) Output signals from the nine-sensor network with one point breakage. (a)–(e) corresponds to breakage at P_1, P_2, P_3, P_4, and P_5, respectively.

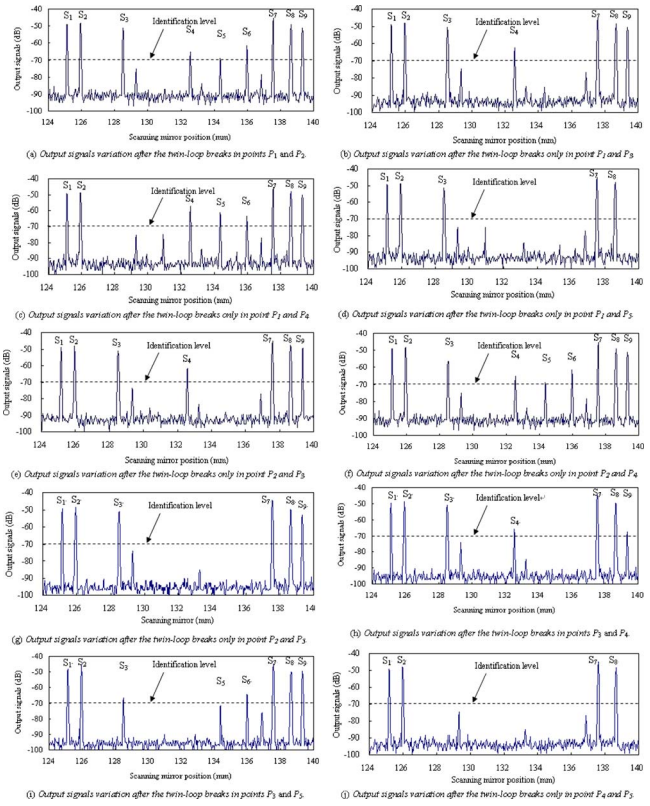

FIG. 8. (Color online) Output signals from the nine-sensor network with two-point breakage. (a)–(j) corresponds, respectively, to the cases of breakages at P_1 and P_2, P_1 and P_3, P_1 and P_4, P_1 and P_5, P_2 and P_3, P_2 and P_4, P_2 and P_5, P_3 and P_4, P_3 and P_5, and P_4 and P_5.

are still maintained above the identification level. When P_3 and P_5 are broken, signal from S_4 disappeared but signals from all other sensors are still there; however, the signal level of S_5 is reduced to slightly below the identification level [Fig. 8(i)]. For the cases of P_1 and P_3 [Fig. 8(g)] P_2 and P_3 [Fig. 8(e)] or P_3 and P_4 [Fig. 8(h)] are broken, all the signals are still there and above the identification level except that the signals from S_5 and S_6 are lost because light from the source cannot reach to these sensors. For the case of P_2 and P_5 being broken [Fig. 8(g)], all the sensor signals from the loop R (S_4, S_5, and S_6) are lost. Signals from four sensors, i.e., S_4, S_5, S_6, and S_9, are lost when P_1 and P_5 are broken [Fig. 8(d)] and five sensor signals (S_3, S_4, S_5, S_6, and S_9) are lost when the broken points are P_4 and P_5 [Fig. 8(j)].

It should be noted that there are "ghost" signals appearing in the output plot, as shown in Fig. 6(b). They are due to unwanted reflections occurring at the fiber joints and the end faces of the fiber sensing segments. These signals are considerably higher than noise floor but significantly lower than the signals from the sensors. By choosing a proper threshold for signal identification, these unwanted peaks should have no effect to the measurement process because they are all below the identification level.

In summary, a multiplexed twin-loop fiber optic sensor network suitable for smart structure applications has been proposed and experimentally tested. The sensor system uses a white light scanning Michelson interferometer as sensor interrogator and can be used to construct sensor networks for distributed strain or temperature measurement in smart structures. Theoretical analysis shows that with a scanning range of 400 nm, it may be possible to multiplex over 100 sensors, assuming that the source power level is sufficiently high. However, for a source power level of 5 mW, due to the

excess insertion losses associated with sensor and joints, the maximum sensor number limited by the power budget requirement is about 28. The twin-loop network architecture greatly improves the reliability of the system by allowing providing redundancy in sensor interrogation by allowing multiple accesses to each sensor in the network. It has been experimentally demonstrated that most of the sensors still function normally even one or two points in the fiber system are broken. Thus helps to reduce the risk of complete system failure due to local damages of sensor-intergraded structures.

ACKNOWLEDGMENTS

This work was supported by the National Natural Science Foundation of China, under Grant No. 60577005 and Specialized Research Fund for the Doctoral Program of Higher Education Institute of MOE, China, to Harbin Engineering University.

[1] A. D. Kersey and W. W. Morey, Electron. Lett. **29**, 112 (1993).
[2] G. Duck and M. M. Ohn, Opt. Lett. **25**, 90 (2000).
[3] E. Sensfelder, J. Burck, and H. J. Ache, Appl. Spectrosc. **52**, 1283 (1998).
[4] V. Lecoeuche, D. J. Webb, C. N. Pannell, and D. A. Jackson, Opt. Commun. **168**, 95 (1999).
[5] L. Yuan and F. Ansari, Sens. Actuators, A **63**, 177 (1997).
[6] L. Yuan and L. Zhou, Appl. Opt. **37**, 4168 (1998).
[7] L. Yuan, L. Zhou, and W. Jin, Opt. Lett. **25**, 1074 (2000).
[8] J. M. Senior, S. E. Moss, and S. D. Cusworth, Opt. Laser Technol. **28**, 1 (1996).
[9] W. Ecke, I. Latka, R. Willsch, A. Reutlinger, and R. Graue, Meas. Sci. Technol. **12**, 974 (2001).
[10] S. A. Al-Chalabi, B. Culshaw, and D. E. N. Davies, *Proceedings of First International Conference on Optical Fiber Sensors*, London, 1983 (unpublished), pp. 132–135.
[11] J. L. Brooks, R. H. Wentworth, R. C. Youngquist, M. Tur, B. Y. Kim, and H. J. Shaw, J. Lightwave Technol. **LT-3**, 1062 (1985).
[12] V. Gusmeroli, J. Lightwave Technol. **11**, 1681 (1993).
[13] W. V. Sorin and D. M. Baney, IEEE Photonics Technol. Lett. **7**, 917 (1995).
[14] D. Inaudi, S. Vurpillot, and S. Lloret, Proc. SPIE **2718**, 251 (1996).
[15] L. Yuan, L. Zhou, W. Jin, and J. Yang, Opt. Lett. **27**, 894 (2002).
[16] L. Yuan, W. Jin, L. Zhou, Y. H. Hoo, and S. M. Demokan, IEEE Photonics Technol. Lett. **14**, 1157 (2002).